this amplifier is synchronised with the response time of OPY such that, as seen in the timing diagram of Fig. 2*b* it is initially maintained into an idle state by the latch signal and, only at the latch control signal, it is activated to drive the output latch shown in Fig. 5.

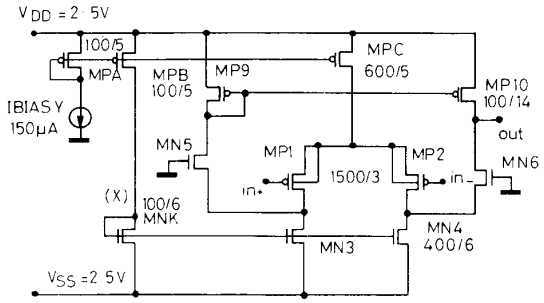

Fig. 3 *Pre-charge amplifier*

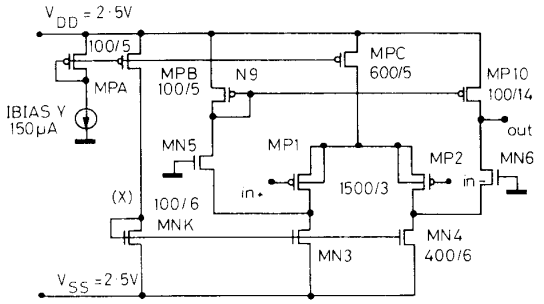

Fig. 4 *Regenerative amplifier*

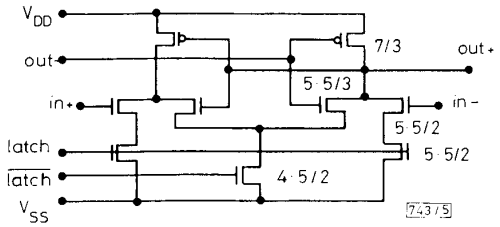

Fig. 5 *Latch*

IC design and experimental results: For a 2 μm CMOS process, the comparator described above has been designed to meet the specifications indicated in Table 1 yielding the transistor ratios shown in the diagrams of Fig. 3 and Fig. 4, respectively for the pre-comparator and regenerative amplifier. The power consumption is 8 mW and the total silicon area is a mere 0·12 mm^2. This comparator has been included in a 16-bit ADC and was shown to perform according to the specifications.[8] In Fig. 6 we can see that the response of the OPY to an input voltage of 500 μV, after having been driven into deep saturation by a −350 mV input voltage, is less than 0·5 μs even in the extreme conditions corresponding to a 10 pF capacitive load of the testing probe. We should notice that, under normal operating conditions, the OPY is loaded by the regenerative amplifier OPW which has an input capacitance of about two orders of magnitude smaller.

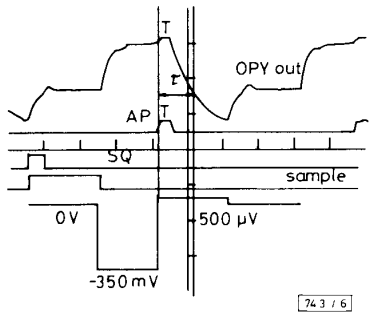

Fig. 6 *Response of OPY to 500 μV after saturation*
10 pF testing probe as load

Table 1 DESIGN SPECIFICATIONS OF THE CMOS VOLTAGE COMPARATOR

Input resolution	±20 μV
Settling time	≤0·75 μs
Auto-zero	≤1 μs
Power dissipation	≤10 mW
Supply voltage	±2·5 V
Area	≈0·10 mm^2

Conclusions: A high performance CMOS comparator was presented which is ideally suited to high resolution A/D conversion because of its low input voltage resolution and fast settling time. The operation of such comparator comprises an auto-reseting phase which significantly reduces the recovery time from saturation and can substantially increase the speed of successive approximation convertors where several consecutive comparisons are performed.

C. A. LEME
J. E. FRANCA
Departamento de Engenharia Electrotécnica e de Computadores
Instituto Superior Técnico
Av. Rovisco Pais, 1096 Lisboa Codex, Portugal

2nd August 1990

References

1 MCCREARY, J., and GRAY, P.: 'All-MOS charge redistribution analog-to-digital conversion techniques — Part I', *IEEE J. Solid-State Circuits*, 1975, **SC-10,** pp. 371–379
2 YEE, Y. S., TERMAN, L. M., and HELLER, L. G.: 'A 1 mV MOS comparator', *IEEE J. Solid-State Circuits*, 1978, **SC-13,** pp. 294–297
3 ENZ, C.: 'Analysis of low-frequency noise reduction by autozero technique', *Electron. Lett.*, 1984, **20,** pp. 959–960
4 SHIEH, J., PATIL, M., and SHEU, B.: 'Measurement and analysis of charge injection in MOS analog switches', *IEEE J. Solid-State Circuits*, 1987, **SC-22,** pp. 277–281
5 GRAY, P. R., and MEYER, R. C.: 'MOS operational amplifier design — A tutorial overview', *IEEE J. Solid-State Circuits*, 1982, **SC-17,** pp. 969–982
6 KLEIN, H. W., and ENGL, W. L.: 'Design techniques for low-noise CMOS operational amplifiers'. ESSCIRC'84 Dig. Tech. Papers, Sept. 1984, pp. 27–30
7 GRAY, P. R., and MEYER, R. C.: 'Analysis and design of analog integrated circuits' (Wiley, New York, 1977)
8 LEME, C. A., and FRANCA, J. E.: 'An overview and novel solutions for high-resolution self-calibrating analogue-digital convertors'. Int. Symp. Signals, Systems and Electronics, Erlangen, Germany, September 18–20, 1989

CONTINUOUS-WAVE HIGH-POWER (75 mW) OPERATION OF A TRANSVERSE-MODE STABILISED WINDOW-STRUCTURE 680 nm AlGaInP VISIBLE LASER DIODE

Indexing term: Semiconductor lasers

75 mW CW output power was obtained for a transverse-mode stabilised window-structure 680 nm AlGaInP visible laser diode with non-absorbing mirror facets formed by disordering of GaInP natural superlattice. Stable fundamental mode operations were achieved at up to 70 mW, which is 2·3 times as high as previously reported.

High-power transverse-mode stabilised AlGaInP visible laser diodes (LDs) have been promising light sources for use in high-density optical disk memory systems, high-speed laser beam printers and many other applications. The output power for AlGaInP LDs under CW fundamental mode operation has

been limited to below 30 mW.[1-4] The limitations are catastrophic optical damage (COD), which occurs because of a thermal runaway caused by lasing light absorption at the mirror facets, and transverse-mode instability at high output power. Window-structure LDs with nonabsorbing mirror facets have been fabricated by various methods and have shown a marked improvement in COD levels for AlGaAs LDs.[5,6] The authors have reported novel window-structure AlGaInP visible LDs formed by disordering of GaInP natural superlattice (NSL)[7,8] and have demonstrated a marked increase in maximum output power under pulsed current operation.[9] This letter reports an improvement in transverse-mode stability for window-structure AlGaInP visible LDs and shows CW maximum output power, 75 mW, and stable fundamental-mode CW operations, up to 70 mW.

Fig. 1 shows a cross-section of the window-structure AlGaInP LD. The LDs were grown on a (001) oriented GaAs

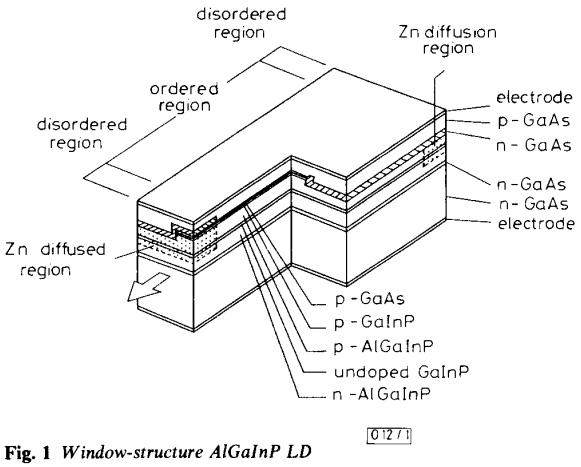

Fig. 1 *Window-structure AlGaInP LD*

substrate by three-step metalorganic vapour phase epitaxy (MOVPE). Growth condition details have been described in Reference 9. The active layer is 60 nm thick undoped $Ga_{0.5}In_{0.5}P$ and the cladding layers are 1 μm thick Zn doped $(Al_{0.6}Ga_{0.4})_{0.5}In_{0.5}P$ and 1 μm thick Si doped $(Al_{0.6}Ga_{0.4})_{0.5}In_{0.5}P$. After the first step MOVPE, the window regions were formed by selective impurity diffusion into the GaInP active layer. Diffused impurity (Zn) disorders the GaInP NSL, which is formed in the active layer during the crystal growth and increases the bandgap energy. Photoluminescence measurements have shown a peak energy shift by 70 meV between the disordered and ordered region. After the selective impurity diffusion, an inverted-mesa stripe was formed in the [110] direction by chemical etching. A 0·20 μm thick *p*-AlGaInP layer was left at the outside of the mesa stripe. The mesa stripe was then buried by an *n*-GaAs blocking layer and covered by a *p*-GaAs contact layer. The mesa stripe provides carrier confinement and forms a refractive-index waveguide along the junction plane. After metallisation, the LDs were cleaved at the disordered regions. The laser cavity was 470 μm long. The ordered region was 400 μm long and the disordered regions at each facet were 30 and 40 μm long. 10% reflectivity and 95% reflectivity facet-coatings were applied to the front and rear facets, respectively.

It has been known that transverse-mode instability for LDs is caused by refractive-index change, caused by injected carrier spatial hole-burning at the transverse-mode peak. A waveguide with a sufficiently large refractive-index step to overcome the refractive-index change is needed for transverse-mode stabilised high-power LDs. A narrow waveguide is also desirable for preventing higher-order transverse-mode lasing and suppressing spatial hole-burning. With the window-structure AlGaInP LDs in this work, the mesa stripe waveguide forms a high effective refractive-index step, 10^{-2}, which is larger than refractive-index changes,[10] several times 10^{-3}, caused by high carrier injection. The waveguide width at the bottom of the mesa is 3 μm, which is less than 60% that for the previously reported high-power AlGaInP LDs.[9]

Fig. 2 shows the light against current (*L/I*) characteristics for a window-structure AlGaInP LD under CW operation at 25°C. 75 mW maximum light output power was achieved. No COD failure was observed. The maximum output power was limited by thermal heating caused by current injection. The threshold current and the wavelength were 90 mA and 680 nm, respectively. Fig. 3 shows the far field patterns at output

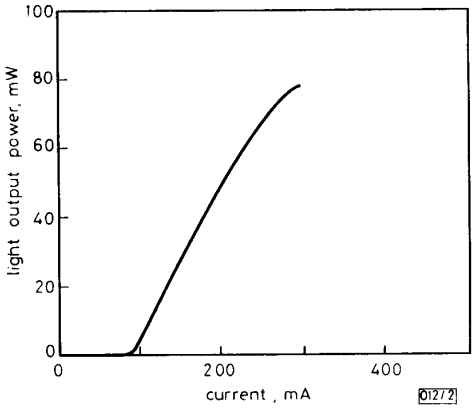

Fig. 2 *Light against current characteristics*
CW 25°C
75 mW output power. COD was not observed
Threshold current = 90 mA; wavelength = 680 nm

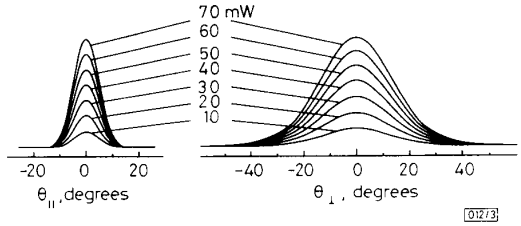

Fig. 3 *Far field patterns for window-structure AlGaInP LD*
CW 25°C
$\theta_{\parallel} = 11°$; $\theta_{\perp} = 30°$. Aspect ratio = 2·7
Maximum output power density > 13 MW/cm^2

powers, ranging from 10 mW to 70 mW. Stable fundamental-mode operations were achieved, up to at least 70 mW. Radiation angles parallel, $\theta_{\parallel}$ and perpendicular, $\theta_{\perp}$, to the junction plane were 11° and 30°, respectively, resulting in a small aspect ratio of 2·7. The maximum output power density at 70 mW is estimated to be more than 13 MW/cm^2.

In summary, 75 mW CW output was obtained for a transverse-mode stabilised window-structure AlGaInP LD at 25°C. Stable fundamental-mode operations were achieved, at least up to 70 mW, which is 2·3 times as high as every reported for AlGaInP LDs. At more than 13 MW/cm^2 output power density, the mirror facet in the disordered region was not catastrophically damaged. The light output power is only thermally limited. These results show that the window-structure significantly improves the maximum CW output power for the transverse-mode stabilised AlGaInP visible LDs.

Acknowledgment: The authors would like to thank M. Sakaguchi and T. Suzuki for their continuous encouragement.

Y. UENO
K. ENDO
H. FUJII
K. KOBAYASHI
K. HARA
T. YUASA

Opto-Electronics Research Laboratories
NEC Corporation
4-1-1, Miyazaki, Miyamae-ku
Kawasaki 213, Japan

17th August 1990

References

1 FUJII, H., KOBAYASHI, K., KAWATA, S., GOMYO, A., HINO, I., HOTTA, H., and SUZUKI, T.: 'High-power operation of a transverse-mode stabilised AlGaInP visible light (λ_L = 683 nm) semiconductor laser', *Electron. Lett.*, 1987, **23**, pp. 938–939

2 KOBAYASHI, K., KAWATA, S., FUJII, H., HINO, I., GOMYO, A., HOTTA, H., and SUZUKI, T.: 'Transverse mode stabilised 670 nm AlGaInP visible-light laser diodes'. Proc. SPIE, Los Angeles, 1988, 898, pp. 84–88
3 ISHIKAWA, M., ITAYA, K., WATANABE, Y., HATAKOSHI, G., SUGAWARA, H., OHBA, Y., and UEMATSU, Y.: 'High power operation of InGaP/InAlP transverse mode stabilized laser diodes'. Extended Abstracts 19th Conf. Solid State Devices and Materials, Tokyo, 1987, pp. 115–118
4 ITAYA, K., WATANABE, Y., ISHIKAWA, M., HATAKOSHI, G., and UEMATSU, Y.: 'High-power operation of heterobarrier blocking structure InGaAlP visible light laser diodes', *Appl. Phys. Lett.*, 1990, **56**, pp. 1718–1719
5 YONEZU, H., UENO, M., KAMEJIMA, T., and HAYASHI, I.: 'An AlGaAs window structure laser', *IEEE J. Quantum Electron.*, 1979, **QE-15**, pp. 775–781
6 SUZUKI, Y., HORIKOSHI, Y., KOBAYASHI, M., and OKAMOTO, H.: 'Fabrication of GaAlAs window-stripe multi-quantum-well heterostructure lasers utilising Zn diffusion-induced alloying', *Electron. Lett.*, 1984, **20**, pp. 383–384
7 GOMYO, A., SUZUKI, T., KOBAYASHI, K., KAWATA, S., and HINO, I.: 'Evidence for the existence of an ordered state in $Ga_{0.5}In_{0.5}P$ grown by metalorganic vapor phase epitaxy and its relation to band-gap energy', *Appl. Phys. Lett.*, 1987, **50**, pp. 673–675
8 GOMYO, A., SUZUKI, T., and IIJIMA, S.: 'Observation of strong ordering in $Ga_xIn_{1-x}P$ alloy semiconductors., *Phys. Rev. Lett.*, 1988, **60**, pp. 2645–2648
9 UENO, Y., FUJII, H., KOBAYASHI, K., GOMYO, A., HARA, K., KAWATA, S., YUASA, T., and SUZUKI, T.: 'Novel window-structure AlGaInP visible-light laser diodes with nonabsorbing facets fabricated by utilizing GaInP natural superlattice disordering', *Jpn. J. Appl. Phys. 2*, 1990, **29**, (9)
10 TANAKA, T., and MINAGAWA, S.: 'Carrier-induced refractive index change, mode gain and spontaneous-emission factor in AlGaInP SQW-SCH laser diodes', *Electron. Lett.*, 1990, **26**, pp. 766–767

EXTENSION OF SPECTRAL DOMAIN APPROACH TO UNILATERAL FINLINES WITH FINITE METALLISATION THICKNESS AND SUBSTRATE SUPPORTING GROOVES

Indexing terms: Millimetre wave integrated circuit, Finline, Planar transmission line, Propagation constant, Characteristic impedance

An extension of the spectral domain approach to characterising the effects of both finite metallisation thickness and substrate supporting groove in unilateral finlines is described. The formulation regards the equivalent magnetic current sheets at the apertures of the groove and on either side of the slot as the source quantities to be determined, which leads to a computationally efficient matrix equation for the propagation constant and the characteristic impedance. A new procedure for deriving the spectral Green's function relating the magnetic fields to the magnetic current sheet at the groove aperture is proposed, where the conventional spectral domain immittance approach is not valid. The results are provided to show how the behaviour of unilateral finlines are affected by the metallisation thickness and substrate supporting groove.

Introduction: Of all the numerical techniques that have evolved for the computation of the frequency-dependent transmission characteristics of finlines, perhaps the most efficient and versatile is the spectral domain approach.[1] This approach has neglected the practical structure details, such as the finite metallisation thickness and the substrate supporting grooves. Recent advances in millimetre wave integrated circuits have created a demand for detailed knowledge of the effects of these parameters. The generalised finlines have been analysed by the mode-matching method including the finite metalisation thickness and substrate supporting grooves[2] and by network analytic methods including the finite metalisation thickness.[3] Chan *et al.* developed a mixed spectral domain approach for the dispersion analysis of finlines considering only substrate supporting grooves.[4] These methods, except that in Reference 3, lead to oversized matrix equations for the accurate solutions. They are primarily oriented towards the computation of propagation constants but rarely concern themselves with the characteristic impedances. This letter describes an extension of spectral domain approach to analysis of frequency-dependent transmission characteristics of unilateral finlines with finite metallisation thickness and substrate supporting grooves. The new features of the formulation include: (*a*) The equivalent magnetic current sheets at the apertures of the groove and on either side of the slot are viewed as the source quantities to be determined. (*b*) A multilevel-filamentary-magnetic-current model for the magnetic current sheet at the groove aperture is presented, which leads to the use of spectral domain approach. (*c*) The expansion coefficient comparison method in cooperation with the application of the inductance theorem is used to derive the spectral Green's functions relating the magnetic fields to the filamentary magnetic currents, where the spectral domain immittance approach is not valid. (*d*) Some new results are provided to demonstrate that both characteristic impedance and propagation constant are dramatically distorted and the parasitic propagating higher order modes will appear when the groove depth becomes larger.

Formulation: Fig. 1 depicts the configuration of the unilateral finline under consideration. Using the equivalence principle,[5]

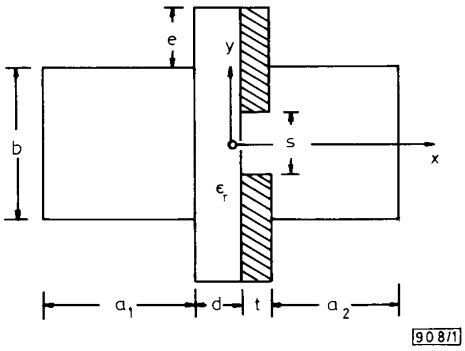

Fig. 1 *Unilateral finline with finite metallisation thickness and substrate supporting groove*

the apertures of the groove, $y = b/2$, and the either side of the slot $x = 0$ and $x = t$, are replaced by the perfectly conducting planes, and at the same time the appropriate magnetic current sheets $\pm\bar{M}_1$, $\pm\bar{M}_2$ and $\pm\bar{M}_3$ are assumed at the corresponding apertures, as shown in Fig. 2. The fields in Fig. 2*a* are equivalent to the sum of the fields radiated by $\bar{M}_1$ and $\bar{M}_3$, and the fields in Fig. 2*b* by $-\bar{M}_1$ and $\bar{M}_2$. The fields in Fig. 2*c* are identical with the fields produced by $-\bar{M}_2$, and the fields in Fig. 2*d* by $-\bar{M}_3$. The direct application of spectral domain approach to Fig. 2 is improper because of the presence of $\pm\bar{M}_3$. To circumvent this restriction, a multilevel-filamentary-magnetic-currents model for $\bar{M}_3$ is presented.

The plane where $\pm\bar{M}_3$ are located is subdivided into N sections. Suppose a filamentary magnetic current at each connection line between adjacent sections. This results in $N - 1$ filamentary magnetic currents. $\bar{M}_3$ is approximated by this set

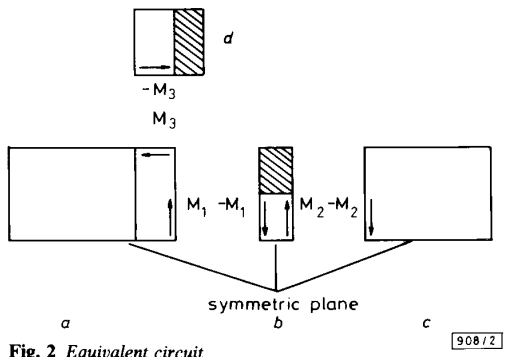

Fig. 2 *Equivalent circuit*